This article was downloaded by: [National Chiao Tung University 國立交通大學]
On: 28 April 2014, At: 05:50
Publisher: Taylor & Francis
Informa Ltd Registered in England and Wales Registered Number: 1072954 Registered office: Mortimer House, 37-41 Mortimer Street, London W1T 3JH, UK

Numerical Heat Transfer, Part A: Applications: An International Journal of Computation and Methodology
Publication details, including instructions for authors and subscription information:
http://www.tandfonline.com/loi/unht20

COMPUTATION OF UNSTABLE LIQUID METAL CONVECTION IN A VERTICAL CLOSED CYLINDER HEATED FROM THE SIDE AND COOLED FROM ABOVE

Y.H. Li [a], K.C. Lin [a] & T.F. Lin [a]
[a] Department of Mechanical Engineering, National Chiao Tung University, Hsinchu, Taiwan
Published online: 12 Mar 2007.

To cite this article: Y.H. Li, K.C. Lin & T.F. Lin (1997) COMPUTATION OF UNSTABLE LIQUID METAL CONVECTION IN A VERTICAL CLOSED CYLINDER HEATED FROM THE SIDE AND COOLED FROM ABOVE, Numerical Heat Transfer, Part A: Applications: An International Journal of Computation and Methodology, 32:3, 289-309, DOI: 10.1080/10407789708913892

To link to this article: http://dx.doi.org/10.1080/10407789708913892

PLEASE SCROLL DOWN FOR ARTICLE

Taylor & Francis makes every effort to ensure the accuracy of all the information (the "Content") contained in the publications on our platform. However, Taylor & Francis, our agents, and our licensors make no representations or warranties whatsoever as to the accuracy, completeness, or suitability for any purpose of the Content. Any opinions and views expressed in this publication are the opinions and views of the authors, and are not the views of or endorsed by Taylor & Francis. The accuracy of the Content should not be relied upon and should be independently verified with primary sources of information. Taylor and Francis shall not be liable for any losses, actions, claims, proceedings, demands, costs, expenses, damages, and other liabilities whatsoever or howsoever caused arising directly or indirectly in connection with, in relation to or arising out of the use of the Content.

This article may be used for research, teaching, and private study purposes. Any substantial or systematic reproduction, redistribution, reselling, loan, sub-licensing, systematic supply, or distribution in any form to anyone is expressly forbidden. Terms & Conditions of access and use can be found at http://www.tandfonline.com/page/terms-and-conditions

Downloaded by [National Chiao Tung University] at 05:50 28 April 2014

COMPUTATION OF UNSTABLE LIQUID METAL CONVECTION IN A VERTICAL CLOSED CYLINDER HEATED FROM THE SIDE AND COOLED FROM ABOVE

Y. H. Li, K. C. Lin, and T. F. Lin
Department of Mechanical Engineering, National Chiao Tung University, Hsinchu, Taiwan

Three-dimensional unsteady numerical computation was carried out to investigate buoyancy-driven unstable convection processes in a side-wall-heated and top-wall-cooled vertical closed cylinder containing liquid metal. The time-dependent basic flow equations were directly solved by the implicit Marker-and-Cell (MAC) scheme with the power law approximation to treat the convection-diffusion couplings. Results were obtained for liquid metal ($Pr = 0.02$) in a cylinder of finite aspect ratio ($\Gamma = 2$) for various Rayleigh numbers. The predicted results indicate that the flow is relatively unstable except at low buoyancy. Specifically, at $Ra = 2000$ the flow evolves to a steady state but is highly asymmetric. As $Ra = 3000$ and 4000, the flow becomes time periodic after the transient has died out with increasing asymmetry. At a still higher buoyancy the oscillation amplitude and flow asymmetry get larger, and a second fundamental frequency appears. The flow is quasi-periodic. Qualitatively, the flow structure is characterized by a main recirculation in the major portion of the cylinder along with two uprising smaller cells near the side wall in the bottom half of the cylinder and another two counterrotating cells in the top half of the cylinder. Finally, the critical Rayleigh number for the transition from a steady to a time periodic state was evaluated.

INTRODUCTION

In recent years there has been a growing interest in using the vertical Bridgman method to grow large bulk crystals for the semiconductor industry. The quality of the crystals grown from this method is known to depend heavily on the thermal buoyancy induced transport processes in the liquid melt, particularly in the vicinity of the melt-crystal interface. The unsteady heat transfer rate in the growing interface resulting from the unstable temperature field driven by a high buoyancy will cause striations in the crystal. Hence a detailed understanding of the buoyancy-driven unstable melt flow and heat transfer in the cylindrical crucibles for growing bulk crystals is rather important in improving quality of the grown

Received 6 January 1997; accepted 31 March 1997.

The financial support of this study by the engineering division of the National Science Council of Taiwan, through contract NSC83-0401-E009-009 is greatly appreciated. The support of the present computation by the National Center for High-Performance Computing and by the Computer Center of the National Chiao Tung University, Taiwan, is also acknowledged.

Address correspondence to Professor Tsing-Fa Lin, Department of Mechanical Engineering, National Chiao Tung University, 1001 Ta Hsueh Road, Hsinchu, Taiwan 30049, Republic of China. E-mail: u801455@cc.nctu.edu.tw

Numerical Heat Transfer, Part A, 32:289–309, 1997
Copyright © 1997 Taylor & Francis
1040–7782/97 $12.00 + .00

NOMENCLATURE

$A(\overline{Nu_t})$	oscillation amplitude of $\overline{Nu_t}$	U, V, W	dimensional velocity components in the radial, azimuthal, and axial directions
B	buoyancy force	VC_{max}	maximum flow speed at selected cross section
d	diameter of cylinder	α	thermal diffusivity
f	oscillation frequency	β	volumetric coefficient of expansion with temperature
g	acceleration due to gravity	Γ	aspect ratio ($= h/d$)
h	height of cylinder	η, ξ	nondimensional coordinates in the radial and axial directions
h_c	convection heat transfer coefficient	μ	viscosity
k	thermal conductivity of fluid	ν	kinematic viscosity
Nu	local Nusselt number	ρ	density
$\overline{Nu_t}$	space averaged Nusselt number	τ_p	nondimensional time period of flow oscillation
P	nondimensional pressure	ϕ	nondimensional temperature
P_m	modified pressure		
Pr	Prandtl number	**Subscripts**	
$q''_w, q''_{w,0}$	heat flux at top and side walls	i, j, k	node indices
r, θ, z	coordinates in the radial, azimuthal, and axial directions	w	wall
Ra	thermal Rayleigh number ($= g\beta q''_{w,0} d^4/k\alpha\nu$)	0	reference quantity
t, τ	dimensional and dimensionless times		
T	temperature		
u, v, w	dimensional velocity components in the radial, azimuthal, and axial directions		

crystals. It is also noted that experimental measurements of the melt flow and temperature are relatively difficult, since the melt flow is normally opaque and at a high temperature. An initial attempt is made in the present study to investigate the detailed transition processes from a stable to an unstable melt flow at an increasing buoyancy through an unsteady three-dimensional numerical simulation. In simulating the melt flow, the interface is assumed to be flat and stationary to facilitate the numerical analysis. The assumption of the stationary interface is appropriate, since the speed of the interface movement during melt growth is much lower than that of the melt flow.

Suitable models to approximate buoyancy-driven convection in various vertical melt growth configurations have been proposed by Müller et al. [1]. When additional convective effects induced by rotation or gradients of surface tension are neglected, the models consist of a vertical cylinder with different thermal boundary conditions. Meanwhile a model experiment was conducted by Müller et al. [1] to visualize the water flow in a cylinder of unit aspect ratio for various thermal conditions covering steady and unsteady convection. Steady and pseudo-steady axisymmetric numerical simulations were carried out by Huang and Hsieh [2] and Lin and Akins [3, 4] to investigate natural convection in a bottom-heated vertical cylinder. Additionally, both the steady axisymmetric and asymmetric flows were predicted for liquid metal (Pr = 0.02) and water (Pr = 6.70) from the three-dimensional numerical simulation [5]. A similar analysis was performed by Neumann [6] for both steady and time-dependent convection. The limits for stable axisymmetric

Downloaded by [National Chiao Tung University] at 05:50 28 April 2014

flow were found, and the effects of the initial thermal condition on the resulting steady flow patterns were examined. The onset of the transient flow oscillation and the induced oscillation frequency were also calculated.

Visualization of a flow for a high Prandtl number fluid (silicone oil with $Pr = 10^5$) in a vertical cylinder heated from below revealed an axisymmetric flow at a slightly supercritical Ra and two distinct three-dimensional flow motions at increasing Ra [7]. Various routes for transition from a steady laminar flow to an unsteady chaotic flow were experimentally determined by Rosenberger and his colleagues [8, 9] for the xenon gas in a bottom heated vertical cylinder. Both the Rulle-Taken and period-doubling routes were reported for different ranges of Ra. A similar experimental study was conducted by Kamotani et al. [10] for gallium melt ($Pr = 0.027$) for both vertical and inclined cylinders. Based on temperature data, various convection flow patterns were inferred.

Asymmetric convection in a vertical cylinder was experimentally found to result from a lack of azimuthal symmetry in the imposed wall temperature by Pulicani et al. [11]. Use of appropriate temperature gradients was experimentally demonstrated to produce a flat interface in the vertical Bridgman growth by Feigelson and Route [12]. Control of the furnace temperature profile near the melt-solid interface was noted to be most effective in producing the flat interface [13].

Instability of silicon melt in the Czochralski configuration was investigated by Kakimoto et al. [14]. Through in situ observation of melt convection and temperature measurement, they noted that in a deeper melt the flow was rather unstable and asymmetric. Their subsequent numerical simulation [15] further suggested that the flow instability also depended critically on the temperature distribution and crystal rotation rate.

The above literature review clearly indicates that the detailed transitional flow structures driven by buoyancy in a vertical cylinder remain largely unexplored, especially for the thermal boundary conditions relevant to the vertical Bridgman growth. More studies are needed to unravel the unstable convection processes in the melt flow contained in a vertical closed cylinder with its side wall heated and top cooled.

MATHEMATICAL FORMULATION

Physical Model

Under consideration is the convection of liquid in a side-wall-heated vertical cylindrical box of height h and diameter d, as schematically shown in Figure 1. Initially, at time $t < 0$ the flow is stationary and isothermal at temperature T_c. At time $t \geqslant 0$ the side wall of the cylinder is subject to a constant heat flux $q''_{w,0}$, and the top wall is maintained at the initial uniform temperature T_c to simulate the top seeding in the vertical Bridgman growth. The bottom wall is thermally well insulated. Numerical experiments are to be conducted here to predict the transitional flow patterns.

Downloaded by [National Chiao Tung University] at 05:50 28 April 2014

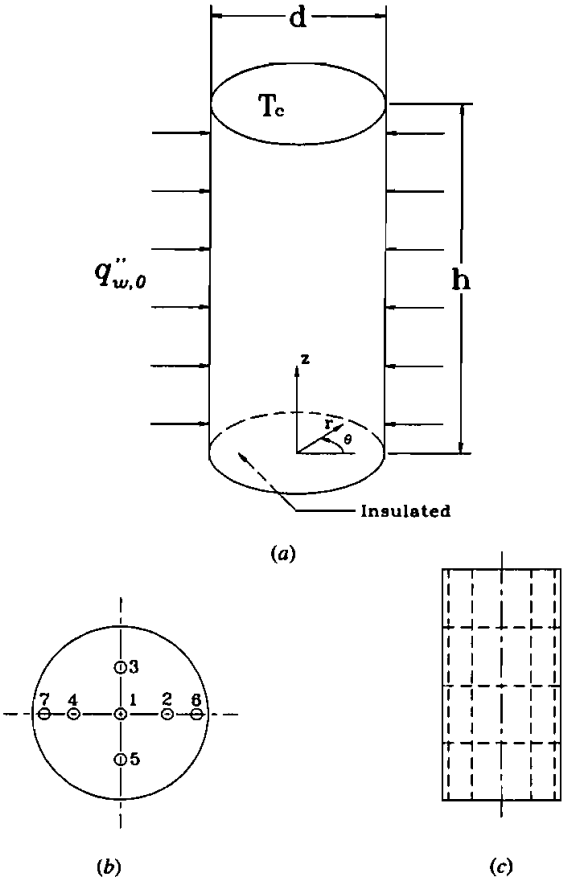

Figure 1. Schematic of the (*a*) physical model and (*b*) top and (*c*) side views of the detection points at all cross sections. Their coordinates are 1 (0, 0, ζ), 2 (0.25, 0, ζ), 3 (0.25, $\pi/2$, ζ), 4 (0.25, π, ζ), 5 (0.25, $3\pi/2$, ζ), 6 [$\frac{1}{2}(1 - 2/I)$, 0, ζ], and 7 [$\frac{1}{2}(1 - 2/I)$, π, ζ], where $\zeta = 0.5$, 1.0, 1.5; I is the total number of nodes in the radial direction.

Under the Boussinesq approximation, basic nondimensional equations describing the flow and thermal evolution in the vertical cylinder are as follows.

Continuity

$$\frac{1}{\eta}\frac{\partial}{\partial \eta}(\eta U) + \frac{1}{\eta}\frac{\partial V}{\partial \theta} + \frac{\partial W}{\partial \xi} = 0 \tag{1}$$

Downloaded by [National Chiao Tung University] at 05:50 28 April 2014

η Momentum

$$\frac{\partial U}{\partial \tau} + U\frac{\partial U}{\partial \eta} + \frac{V}{\eta}\frac{\partial U}{\partial \theta} - \frac{V^2}{\eta} + W\frac{\partial U}{\partial \xi}$$

$$= -\frac{\partial P}{\partial \eta} + \mathrm{Pr}\left\{\frac{\partial}{\partial \eta}\left[\frac{1}{\eta}\frac{\partial}{\partial \eta}(\eta U)\right] + \frac{1}{\eta^2}\frac{\partial^2 U}{\partial \theta^2} - \frac{2}{\eta^2}\frac{\partial V}{\partial \theta} + \frac{\partial^2 U}{\partial \xi^2}\right\} \tag{2}$$

θ Momentum

$$\frac{\partial V}{\partial \tau} + U\frac{\partial V}{\partial \eta} + \frac{V}{\eta}\frac{\partial V}{\partial \theta} + \frac{UV}{\eta} + W\frac{\partial V}{\partial \xi}$$

$$= -\frac{1}{\eta}\frac{\partial P}{\partial \theta} + \mathrm{Pr}\left\{\frac{\partial}{\partial \eta}\left[\frac{1}{\eta}\frac{\partial}{\partial \eta}(\eta V)\right] + \frac{1}{\eta^2}\frac{\partial^2 V}{\partial \theta^2} + \frac{2}{\eta^2}\frac{\partial U}{\partial \theta} + \frac{\partial^2 V}{\partial \xi^2}\right\} \tag{3}$$

ξ Momentum

$$\frac{\partial W}{\partial \tau} + U\frac{\partial W}{\partial \eta} + \frac{V}{\eta}\frac{\partial W}{\partial \theta} + W\frac{\partial W}{\partial \xi}$$

$$= -\frac{\partial P}{\partial \xi} + \mathrm{Pr}\left\{\frac{1}{\eta}\frac{\partial}{\partial \eta}\left(\eta\frac{\partial W}{\partial \eta}\right) + \frac{1}{\eta^2}\frac{\partial^2 W}{\partial \theta^2} + \frac{\partial^2 W}{\partial \xi^2}\right\} + \mathrm{Ra}\,\mathrm{Pr}\,\phi \tag{4}$$

Energy

$$\frac{\partial \phi}{\partial \tau} + U\frac{\partial \phi}{\partial \eta} + \frac{V}{\eta}\frac{\partial \phi}{\partial \theta} + W\frac{\partial \phi}{\partial \xi}$$

$$= \frac{1}{\eta}\frac{\partial}{\partial \eta}\left(\eta\frac{\partial \phi}{\partial \eta}\right) + \frac{1}{\eta^2}\frac{\partial^2 \phi}{\partial \theta^2} + \frac{\partial^2 \phi}{\partial \xi^2} \tag{5}$$

Downloaded by [National Chiao Tung University] at 05:50 28 April 2014

The above equations are written in terms of the following nondimensional variables:

$$\eta = \frac{r}{d} \qquad \xi = \frac{z}{d} \qquad \theta = \theta$$

$$U = \frac{u}{\alpha/d} \qquad V = \frac{v}{\alpha/d} \qquad W = \frac{w}{\alpha/d}$$

$$P = \frac{P_m}{\rho_0(\alpha^2/d^2)} \qquad \phi = \frac{T - T_c}{q''_{w,0}d/k} \qquad \Gamma = \frac{h}{d}$$

$$\mathrm{Pr} = \frac{\nu}{\alpha} \qquad \mathrm{Ra} = \frac{g\beta q''_{w,0}d^4}{k\alpha\nu} \qquad \tau = \frac{t}{d^2/\alpha}$$

and are subject to the following initial and boundary conditions:

For $\tau < 0$

$$U = V = W = \phi = 0$$

For $\tau \geqslant 0$

$$\begin{aligned} &\text{at } \eta = \frac{1}{2}: && U = V = W = -\frac{\partial\phi}{\partial\eta} + 1 = 0 \\ &\text{at } \xi = 0: && U = V = W = \frac{\partial\phi}{\partial\xi} = 0 \\ &\text{at } \xi = \Gamma: && U = V = W = \phi = 0 \end{aligned} \tag{6}$$

It should be mentioned that the viscous dissipation in the melt flow is insignificant compared with that supplied externally [16], and hence it is neglected in the energy equation.

Local and Average Nusselt Numbers

The local heat flux q''_w from the fluid to the isothermal top wall can be expressed as $q''_w = h_c(T - T_c)$, where q''_w is evaluated from the temperature field as $q''_w = -k(\partial T/\partial z)|_{z=h}$. The local Nusselt number is defined as

$$\mathrm{Nu} = \frac{h_c d}{k} \tag{7}$$

and the space averaged Nusselt number is evaluated by

$$\overline{\mathrm{Nu}_t} = \frac{1}{(\pi d^2/4)} \int_{r=0}^{d/2} \int_{\theta=0}^{2\pi} \mathrm{Nu}\, r\, d\theta\, dr \tag{8}$$

Downloaded by [National Chiao Tung University] at 05:50 28 April 2014

SOLUTION METHOD

In view of the nonlinearity in the governing differential equations, the problem is solved numerically by a finite difference method in this study. After comparing various numerical schemes for incompressible flow computation, the implicit Marker-and-Cell (MAC) method developed by Harlow and Welch [17] was chosen to solve the flow equations in primitive form on a staggered grid to exploit the direct coupling of the flow and pressure fields in it. In particular, the unsteady terms were treated by the fully implicit first-order Euler approximation, and the combined convective and diffusive terms were approximated by a power law scheme [18]. At each time step the discretized flow equations derived from integrating Eqs. (2)–(5) over the control volumes for all nodes in the computation grid were solved simultaneously with the Poisson pressure equation:

$$\nabla^2 P = -\nabla \cdot (\mathbf{V} \cdot \nabla)\mathbf{V} - \frac{\partial(\nabla \cdot \mathbf{V})}{\partial \tau} + \mathrm{Pr}\,\nabla^2(\nabla \cdot \mathbf{V}) + \nabla \cdot \mathbf{B} \tag{9}$$

where $\mathbf{V}$ is the velocity vector, $\mathbf{B}$ the buoyancy force, and ∇ the gradient operator. A uniform grid was employed in the computation. In the θ and ξ directions, 40 and 60 nodes were used, respectively. The number of nodes deployed in the radial direction ranges from 30 to 80 depending on the Ra of the flow. The time interval $\Delta\tau$ was chosen to be in the range of 10^{-4} to 10^{-3}.

In a cylindrical domain encountered here, singularity of the basic flow equations at the cylinder axis ($r = 0$) needs to be overcome. This singularity is avoided by placing the temperature node at $r = 0$ in the staggered grid instead of the velocity components. Then the energy equation is integrated over a control volume for this temperature node. The divergence theorem [19] is used to transform the volume integral into a surface integral. Thus the combined conductive and convective energy flux needs to be evaluated only at the control surface that surrounds the cylinder axis, and the singularity is prevented.

Computation was started from the initiation of the transient at $\tau = 0$ to the final steady state or to the statistically stable state when the flow does not become steady at long times. The convergence criteria for U, V, W, P, and ϕ at each time step were

$$\frac{\sum_{i,j,k} |\zeta_{i,j,k}^{m+1} - \zeta_{i,j,k}^{m}|}{\max|\zeta^{m+1}|[(I \cdot J + 1)K]} < 10^{-3} \tag{10}$$

where I, J, and K are the total number of nodes in the η, θ, and ξ directions, respectively, and ζ^{m+1} denotes U, V, W, P, or ϕ at the $(m + 1)$th iteration. Moreover, the flow is considered to have reached steady state when the relative differences in ζ between two consecutive time steps are below 10^{-6}.

Since no analytical solution is available for three-dimensional natural convection in a confined box, it is necessary to compare our numerical results with previously published data to ensure the accuracy of the proposed solution method.

Downloaded by [National Chiao Tung University] at 05:50 28 April 2014

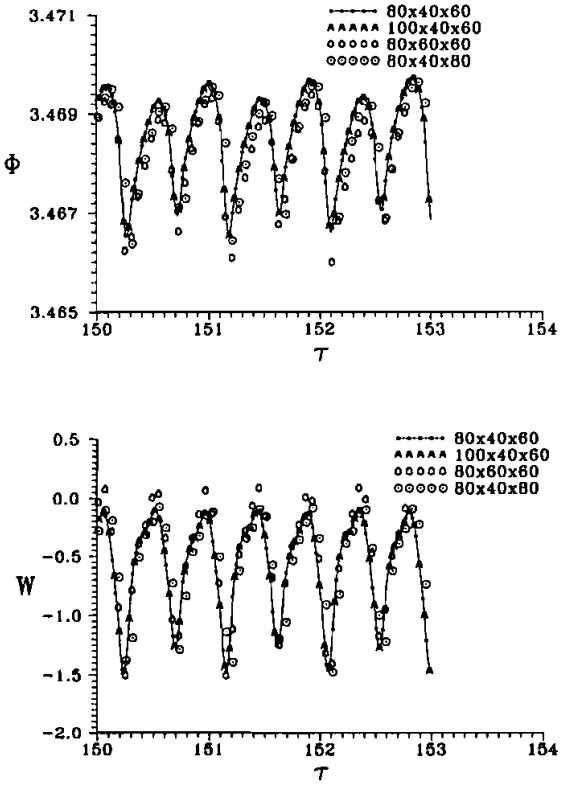

Figure 2. Comparison of ϕ and W variations with time at (0, 0, 0.5) for Pr = 0.02, Γ = 2, and Ra = 4000 computed from various grids.

The predicted steady flow structure for a vertical cylinder heated from below with an insulated side wall for Pr = 6.7, Ra = 2800, and Γ = 0.5 was compared with that from flow visualization and numerical computation by Müller et al. [5], and the agreement is good. A grid-independence test was conducted next. Figure 2 compares sampled results from this test for the time variations of temperature and axial velocity at a selected location (0, 0, 0.5) for a typical periodic case with Pr = 0.02, Ra = 4000, and Γ = 2 computed from four different grids 80 × 40 × 60, 100 × 40 × 60, 80 × 60 × 60, and 80 × 40 × 80 with $\Delta\tau = 10^{-3}$. The agreement is also good. Due to the limited availability of the computational facility, grids much finer than those used were not tested. Through these programs tests the solution method is considered to be suitable for the present problem.

RESULTS AND DISCUSSION

The previous mathematical formulation indicates that the flow to be investigated is governed by three nondimensional parameters, namely, the Prandtl number Pr, Rayleigh number Ra, and aspect ratio Γ. In this study, Γ is fixed at 2 and

Downloaded by [National Chiao Tung University] at 05:50 28 April 2014

the liquid Pr is chosen to be 0.02 (liquid metal). Only Ra is varied from a low value at which the flow is steady to a high value at which the flow is highly unstable to reveal the transition from a steady to unsteady buoyancy-driven flow.

Results from this computation indicate that the flow can evolve to a steady state only at a very low Ra. The critical Ra for the flow to bifurcate from a steady to a time-dependent state is discussed below. Figure 3 presents the predicted steady three-dimensional velocity vector map at a low buoyancy for Ra = 2000. Note that even at this low Ra, the induced flow is highly nonsymmetric and contains highly distorted vortices. More specifically, the flow consists of a main recirculation sinking along the side wall around $\theta = 90°$ and rising along the

Downloaded by [National Chiao Tung University] at 05:50 28 April 2014

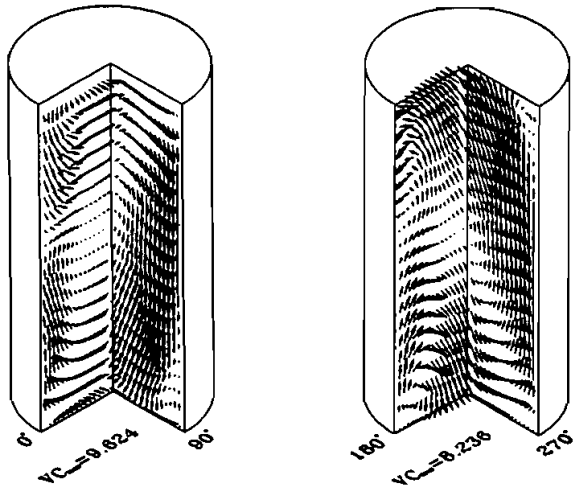

(*a*)

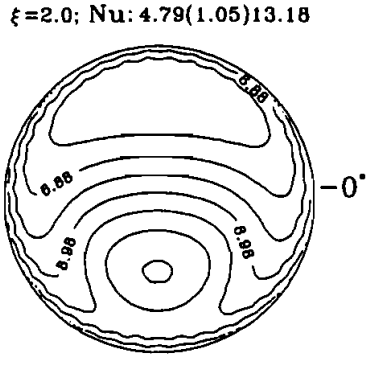

(*b*)

Figure 3. (*a*) Three-dimensional velocity vectors at selected planes and (*b*) local Nusselt number distribution at $\tau = 170$ for Pr = 0.02, Ra = 2000, and $\Gamma = 2$.

opposite side wall near $\theta = 270°$. This recirculation is highly distorted with the flow near the side wall at $\theta = 0°$ and 180° respectively ascending in the bottom half of the cylinder and descending in the top half.

This complex flow requires careful examination. A closer inspection of the flow reveals that the downward flow along the side wall near $\theta = 90°$ can be also deflected toward $\theta = 0°$ and 180° when hitting the bottom wall, in addition to directly reversing its direction to move up along the side wall near $\theta = 270°$. Similar flow deflection is noted on the top wall for the upward flow near $\theta = 270°$. Thus the flows in the top and bottom halves of the cylinder near $\theta = 0°$ and 180° are in the opposite direction. The resulting steady local Nu distribution (Figure 3*b*) on the top plate is rather nonuniform, and the steady average Nu is 8.22.

Results for higher buoyancies are examined next. As the thermal Ra is raised to 3000, the flow was found to gradually evolve to a time periodic state. At this higher Ra the overall flow structure resembles that at Ra = 2000, but the induced recirculating flow is slightly stronger and is distorted to a larger degree, as is evident from the velocity vector plots and isotherms at selected vertical planes at three selected time steps in a typical periodic cycle shown in Figure 4. In this figure, τ denotes a certain time instant when the flow has already evolved to a time periodic state. Note that in a periodic cycle there is significant velocity oscillation with time and the main recirculation also moves slightly up and down with time. The associated local Nu given in Figure 5 are also higher and more nonuniform. In addition, the space averaged Nu variation with time $\overline{\mathrm{Nu}}_t$ (Figure 5) and the time records of the calculated liquid temperature ϕ and vertical velocity component W at selected locations specified in Figure 1 (Figure 6) indicate that the entire flow oscillates at a single fundamental frequency $f_1 = 0.933$ and its harmonics. Also note that the amplitude of the vertical velocity oscillation is much larger than the temperature oscillation. Moreover, a significant variation in the velocity oscillation amplitude with the space location is noted. Specifically, in certain regions around locations 2 and 4 between the cylinder axis and side wall the flow oscillation is much larger and the temperature oscillation slightly higher. Near the side wall at locations 6 and 7 the flow oscillation is rather weak. Furthermore, at the midheight of the cylinder ($\xi = 1.0$) the flow oscillation is much weaker.

For a further raise of Ra to 4000 the resulting flow strengthens slightly and also oscillates periodically in time at a higher frequency $f_1 = 1.133$ ($\tau_p = 0.882$). In addition, the flow structure is in a larger distortion. Obviously, the local Nu is more nonuniform and the space averaged Nu oscillates with a larger amplitude. The time records for ϕ and W and their power spectrum densities are similar to those in Figure 6 for Ra = 3000 except that the oscillation frequency and amplitude are slightly higher.

Now as Ra is raised to 5000, the main flow recirculation also slowly rotates clockwise around the cylinder axis, as reflected in the local Nu distributions at various instants in time (Figure 7). Hence a significant change in the flow structure occurs when Ra is raised from 4000 to 5000. More specifically, the three-dimensional velocity and temperature fields in a periodic cycle shown in Figure 8 indicate that in the top half of the cylinder the flow ascends along the side wall around the planes $\theta = 0°$ and 90° and descends near the planes at $\theta = 180°$ and 270° at time τ. There is a small recirculation around the plane $\theta = 90°$ near the top corner. Later

Downloaded by [National Chiao Tung University] at 05:50 28 April 2014

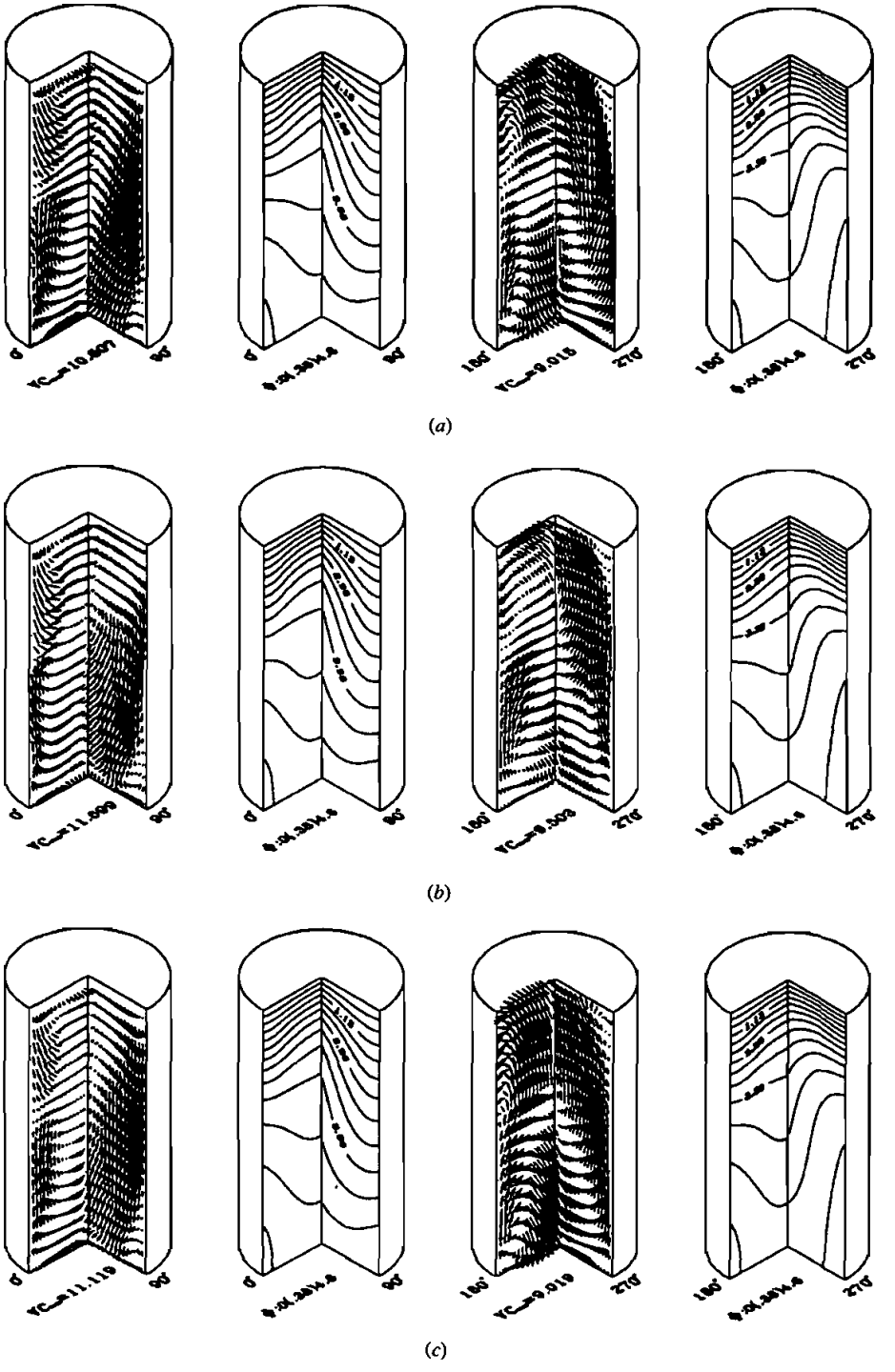

Figure 4. Three-dimensional velocity vectors and temperature contours at three selected time instants—(*a*) τ, (*b*) $\tau + \frac{1}{3}\tau_p$, (*c*) $\tau + \frac{2}{3}\tau_p$—in a periodic cycle for Pr = 0.02, Ra = 3000, and $\Gamma = 2$ ($\tau_p = 1.07$).

Downloaded by [National Chiao Tung University] at 05:50 28 April 2014

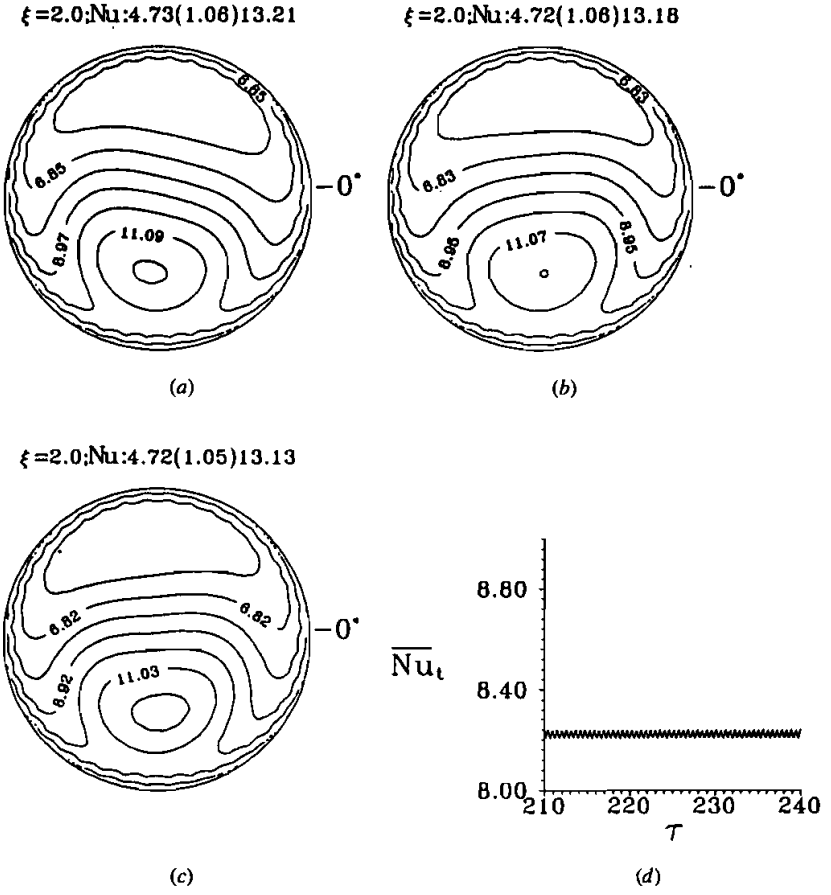

Figure 5. Local Nusselt number distributions at three time instants: (*a*) τ, (*b*) $\tau + \frac{1}{3}\tau_p$, (*c*) $\tau + \frac{2}{3}\tau_p$ and (*d*) average Nusselt number variation with time for Pr = 0.02, Ra = 3000, and $\Gamma = 2$ ($\tau_p = 1.07$).

at $\tau + \frac{1}{3}\tau_p$ the flow mainly moves downward on the planes $\theta = 0°$ and 90° and upward on the plane $\theta = 270°$. In addition, a recirculation now appears on the plane $\theta = 180°$ near the top corner. Then at $\tau + \frac{2}{3}\tau_p$ the flow sinks on the planes $\theta = 0°$ and 270° and rises on the plane $\theta = 180°$, and a small recirculation is seen near the plane $\theta = 0°$ in the bottom corner. Checking with the time variation of $\overline{Nu_t}$ in Figure 7 and time records of ϕ and W, given below, reveals that at Ra = 5000 the temperature oscillation is characterized by a low-amplitude high-frequency component superimposed on a high-amplitude low-frequency component in a periodic cycle ($\tau_p = 66$). In fact, there are two fundamental frequencies in the oscillation, $f_1 = 1.316$ and $f_2 = 0.015$. Hence the flow is quasi-periodic. For the velocity oscillation the amplitude of the high-frequency component is also rather large. Also, at this higher Ra the oscillation at all detection points is large.

Downloaded by [National Chiao Tung University] at 05:50 28 April 2014

Downloaded by [National Chiao Tung University] at 05:50 28 April 2014

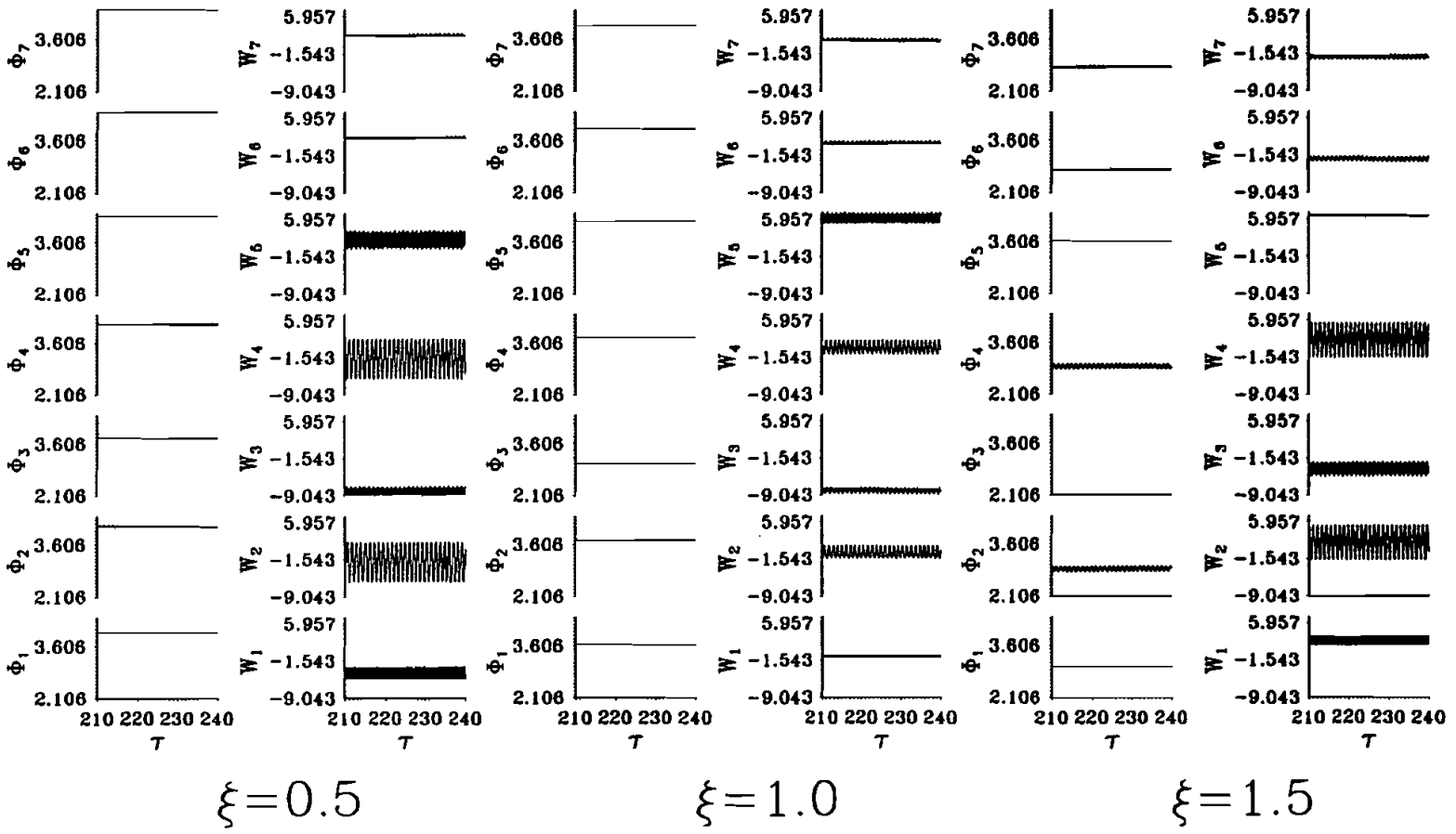

Figure 6. Temperature ϕ and vertical velocity W variations with time at selected tracing points specified in Figure 1 at $\xi = 0.5$, 1.0, and 1.5 for Pr = 0.02, Ra = 3000, and $\Gamma = 2$ (ϕ_i and W_i denote values of ϕ and W at location i).

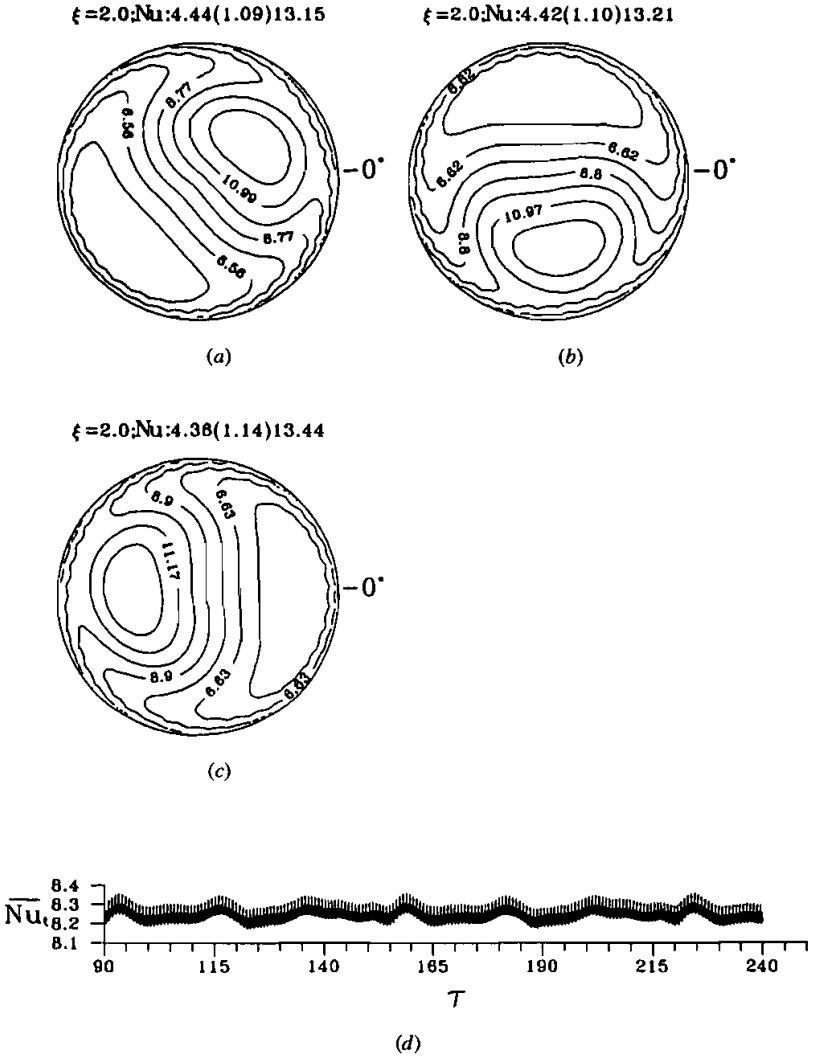

Figure 7. Local Nusselt number distributions at three time instants: (*a*) τ, (*b*) $\tau + \frac{1}{3}\tau_p$, (*c*) $\tau + \frac{2}{3}\tau_p$ and (*d*) average Nusselt number variation with time for Pr = 0.02, Ra = 5000, and $\Gamma = 2$ ($\tau_p = 66$).

At still higher Ra of 6000 and 7000 the induced flow is still quasi-periodic and is qualitatively similar to that for Ra = 5000. Change in the induced flow structures with time is more significant (Figure 9). Specifically, the flow oscillation is also in the form of a high-frequency low-amplitude component superimposed on a low-frequency high-amplitude component, as is clear from the time histories of ϕ and

Downloaded by [National Chiao Tung University] at 05:50 28 April 2014

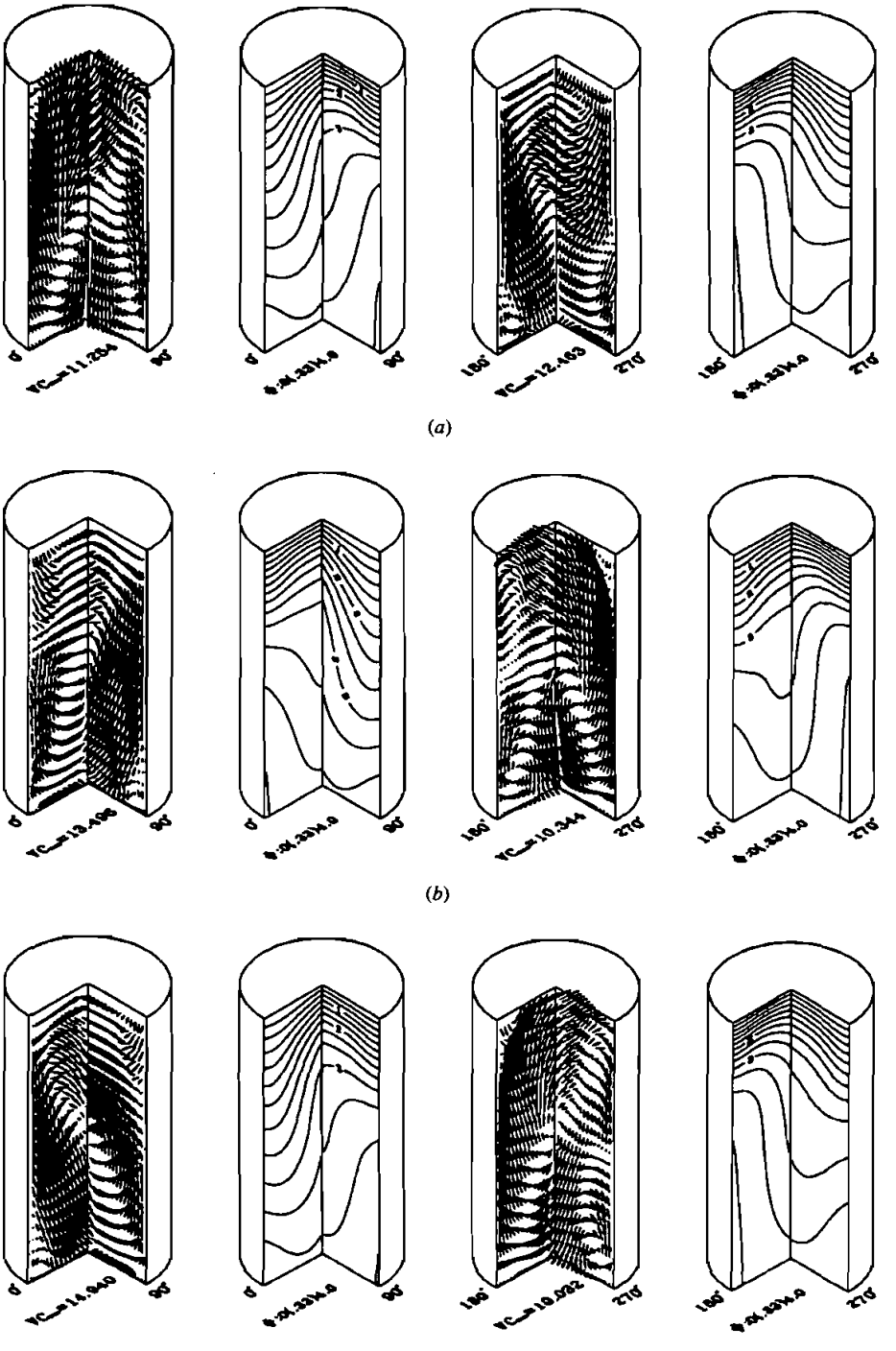

Figure 8. Three-dimensional velocity vectors and isotherms at three selected time instants—(*a*) τ, (*b*) $\tau + \frac{1}{3}\tau_p$, (*c*) $\tau + \frac{2}{3}\tau_p$—in a periodic cycle for Pr = 0.02, Ra = 5000, and $\Gamma = 2$ ($\tau_p = 66$).

Downloaded by [National Chiao Tung University] at 05:50 28 April 2014

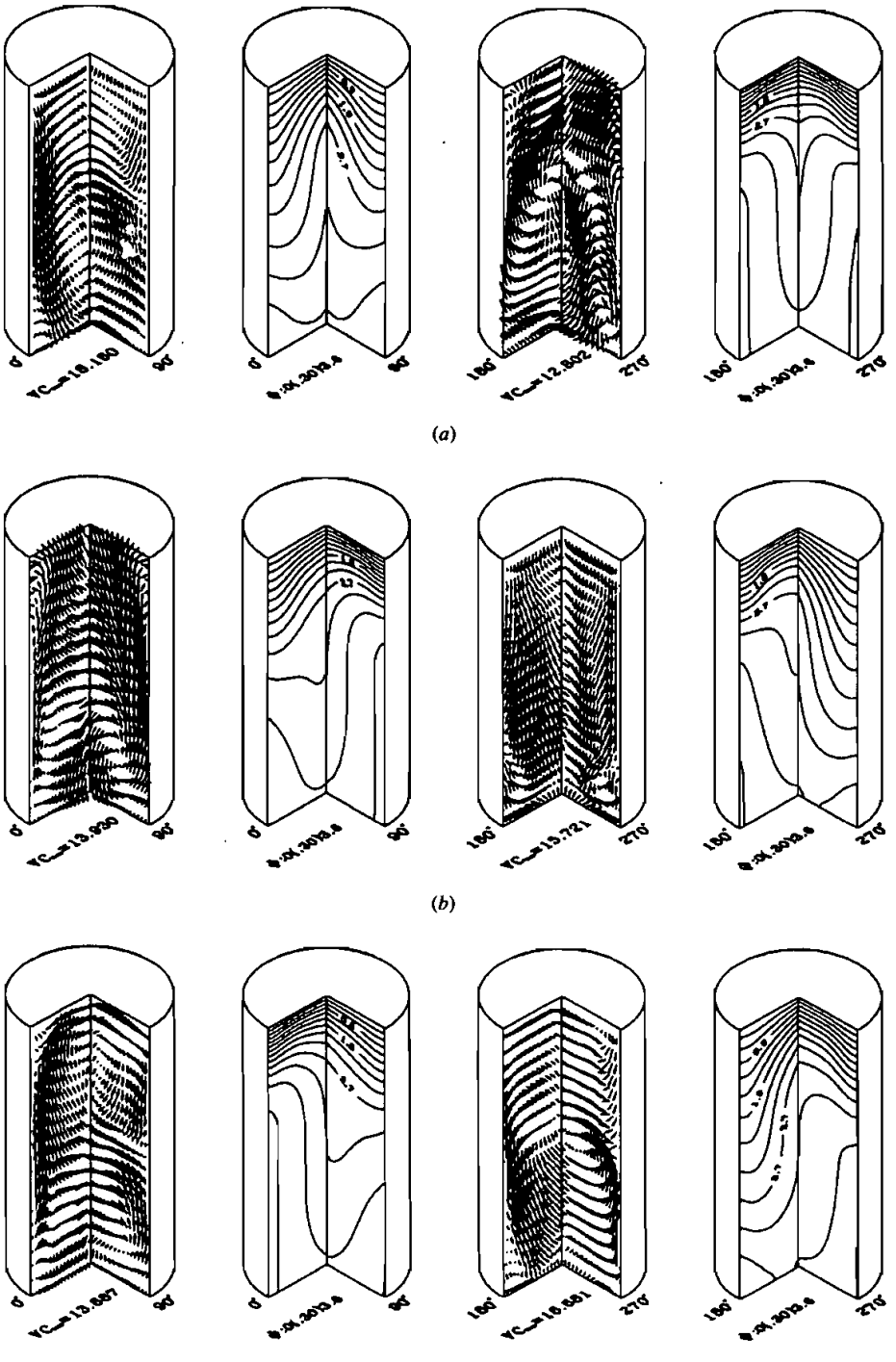

(a)

(b)

(c)

Figure 9. Three-dimensional velocity vectors and isotherms at three selected time instants—(*a*) τ, (*b*) $\tau + \frac{1}{3}\tau_p$, (*c*) $\tau + \frac{2}{3}\tau_p$—in a periodic cycle for Pr = 0.02, Ra = 7000, and $\Gamma = 2$ ($\tau_p = 42$).

Downloaded by [National Chiao Tung University] at 05:50 28 April 2014

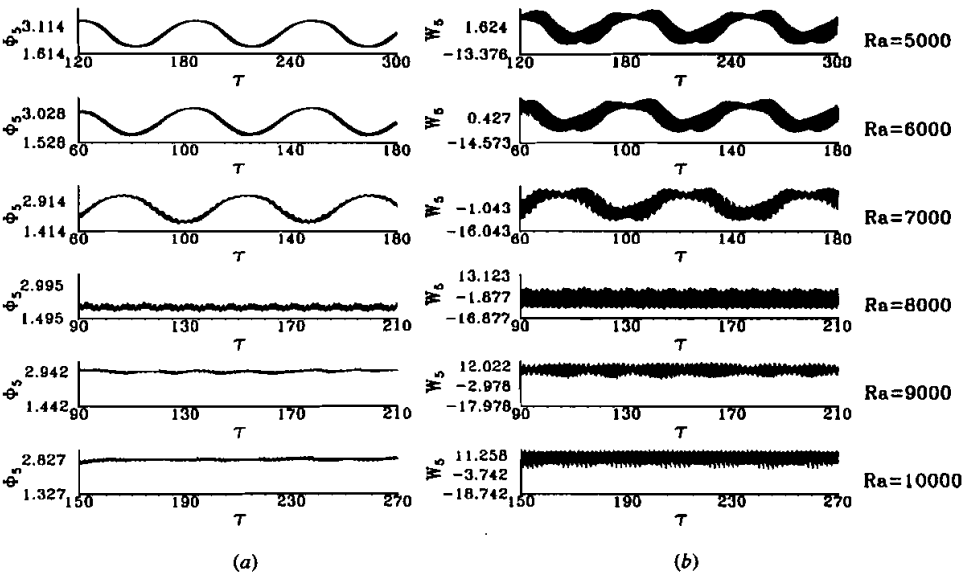

Figure 10. Time records of (*a*) ϕ and (*b*) W at detection point 5 at $\xi = 1.5$ for Pr = 0.02 and $\Gamma = 2$ for various Ra.

W at location 5 given in Figure 10 for Ra = 5000–10,000. According to the power spectrum density analysis of these data, the flow oscillation also consists of two widely spaced fundamental frequencies $f_1 = 1.54$ and $f_2 = 0.024$ for Ra = 6000 and $f_1 = 1.63$ and $f_2 = 0.024$ for Ra = 7000. The corresponding local and average Nusselt numbers also resemble those for Ra = 5000.

When Ra is raised further to 8000, 9000, and 10,000, the flow is also characterized by two fundamental frequencies (Figure 10). But these two frequencies are a little closer. For Ra = 8000, 9000, and 10,000 the two frequencies are 0.533 and 0.133, 0.550 and 0.058, and 0.633 and 0.067, respectively. These quasi-periodic flow oscillations are also seen in the time variations of the average Nu for these cases (Figure 11). An even larger change in the flow structure with time was noted in Figure 12 for Ra = 10,000.

On the basis of the present data, the critical Rayleigh number Ra_c for the transition from steady to unsteady states (the Hopf bifurcation) is approximately determined by plotting the variation of the oscillation amplitude of $\overline{\mathrm{Nu}_t}$ and by extrapolating the fitting curves to the horizontal axis. The result is shown in Figure 13, and Ra_c is about 2186. A direct computation of the case for Ra = 2186 indicated that the oscillation amplitude of $\overline{\mathrm{Nu}_t}$ at long times is extremely small with $A(\overline{\mathrm{Nu}_t}) \approx 4 \times 10^{-6}$. Thus the above extrapolated Ra_c is rather accurate.

CONCLUDING REMARKS

Through a three-dimensional unsteady numerical simulation, effects of thermal buoyancy on the transitional flow and heat transfer in a vertical cylinder

Downloaded by [National Chiao Tung University] at 05:50 28 April 2014

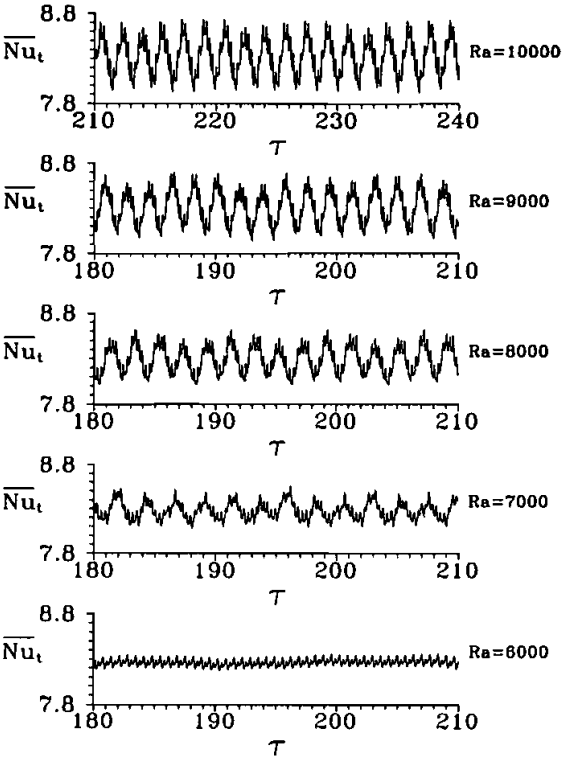

Figure 11. Average Nusselt number variations with time for Pr = 0.02 and Γ = 2 for various Ra.

(Γ = 2) with its side wall heated and top wall cooled are investigated. Computations were carried out for a liquid metal with Pr = 0.02 for various Ra. Results indicate that the flow is relatively unstable. Specifically, at Ra = 2000 the resulting flow is steady but asymmetric. As Ra reaches 3000 the flow already becomes time periodic and oscillates in a large amplitude. At increasing Ra the oscillation amplitude is larger. For Ra = 5000–7000 the flow oscillation is in the form of a small-amplitude high-frequency component superimposed on a large-amplitude low-frequency component. Thus the flow oscillates at two widely different frequencies. For Ra $\geqslant$ 8000 we also observed two fundamental frequencies in the flow oscillation, but their values are not so distant. The oscillation amplitude is rather large.

Qualitatively, the induced flow structure consists of a main recirculation in the major portion of the cavity and four smaller cells resulting from the deflecting flow at the cylinder top and bottom to move in all directions. Thus, on each side of the main circulation the two cells are counterrotating. At high Ra the flow also rotates slowly around the cylinder axis.

Downloaded by [National Chiao Tung University] at 05:50 28 April 2014

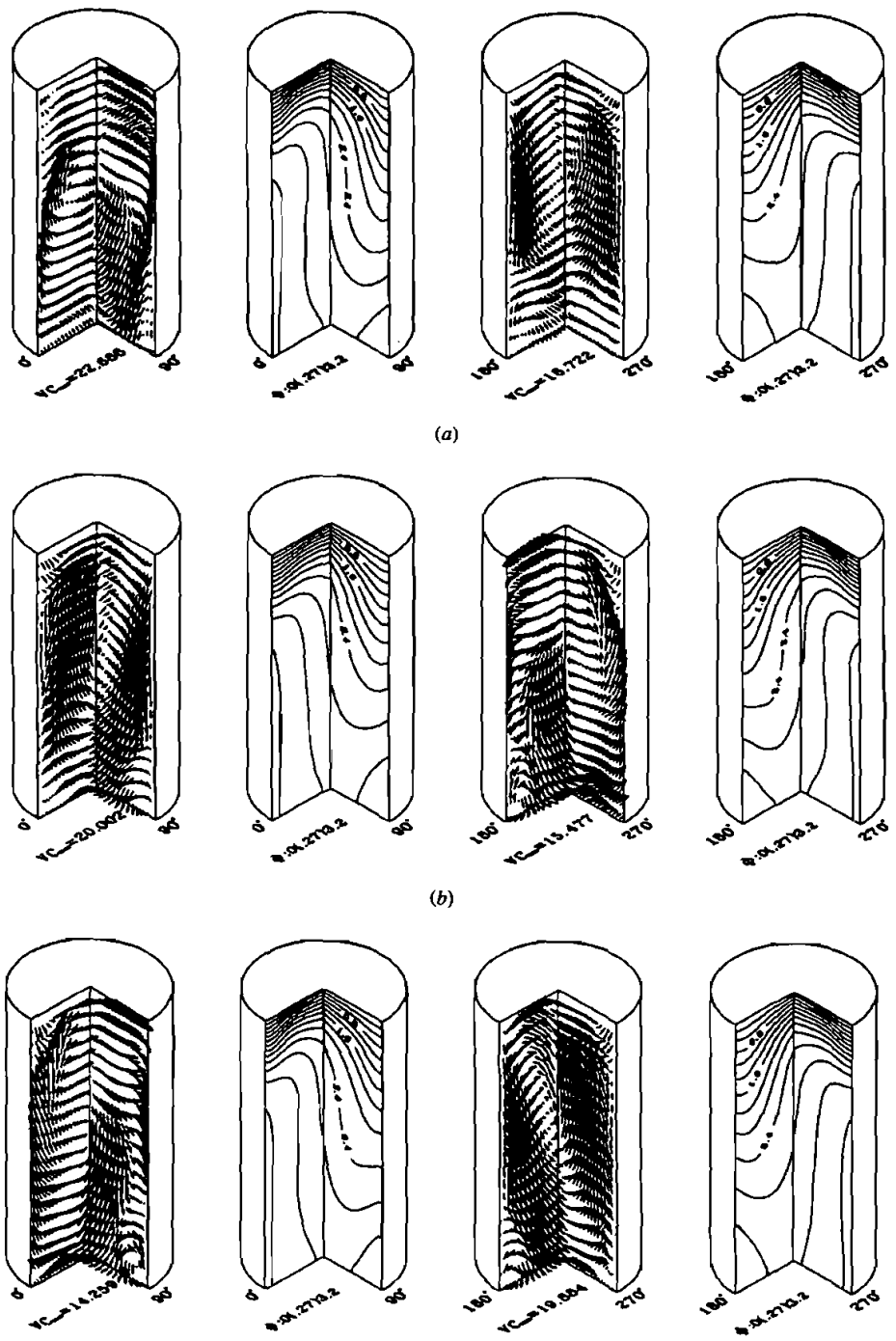

Figure 12. Three-dimensional velocity vectors and isotherms at three selected time instants—(*a*) τ, (*b*) $\tau + \frac{1}{3}\tau_p$, (*c*) $\tau + \frac{2}{3}\tau_p$—in a periodic cycle for Pr = 0.02, Ra = 10,000, and $\Gamma = 2$ ($\tau_p = 15$).

Downloaded by [National Chiao Tung University] at 05:50 28 April 2014

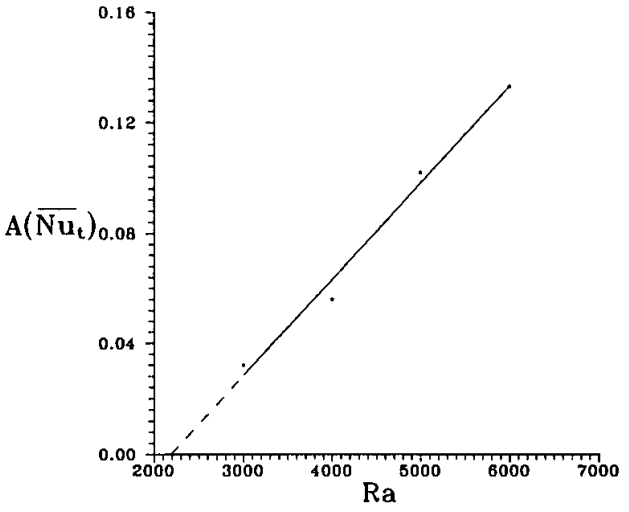

Figure 13. Oscillation amplitudes of average Nusselt number $\overline{Nu_t}$ at various Ra and extrapolation to find the critical Rayleigh number for onset of flow oscillation.

During the course of this investigation it is realized that a method like crucible rotation is often used to stabilize the buoyancy-driven time-dependent flow and needs to be examined in detail in the future.

REFERENCES

1. G. Müller, G. Neumann, and H. Matz, A Two-Rayleigh-Number Model of Buoyancy-Driven Convection in Vertical Melt Growth Configurations, *J. Cryst. Growth*, vol. 84, pp. 36–49, 1987.
2. D. Y. Huang and S. S. Hsieh, Analysis of Natural Convection in a Cylinder Enclosure, *Numer. Heat Transfer*, vol. 12, pp. 121–135, 1987.
3. Y. S. Lin and R. G. Akins, Pseudo-Steady-State Natural Convection Heat Transfer Inside a Vertical Cylinder, *Trans. ASME J. Heat Transfer*, vol. 108, pp. 310–316, 1986.
4. Y. S. Lin and R. G. Akins, Thermal Description of Pseudo-Steady-State Natural Convection Inside a Vertical Cylinder, *Int. J. Heat Mass Transfer*, vol. 29, pp. 301–307, 1986.
5. G. Müller, G. Neumann, and W. Weber, Natural Convection in Vertical Bridgman Configurations, *J. Cryst. Growth*, vol. 70, pp. 78–93, 1984.
6. G. Neumann, Three-Dimensional Numerical Simulation of Buoyancy-Driven Convection in Vertical Cylinders Heated from Below, *J. Fluid Mech.*, vol. 214, pp. 559–578, 1990.
7. R. S. Figliola, Convection Transitions Within a Vertical Cylinder Heated from Below, *Phys. Fluids*, vol [illegible] no. 7, pp. 2028–2031, 1986.
8. J. M. Olson and F. Rosenberger, Convective Instabilities in a Closed Vertical Cylinder Heated from Below, Part 1, Monocomponent Gases, *J. Fluid Mech.*, vol. 92, pp. 609–629, 1978.

Downloaded by [National Chiao Tung University] at 05:50 28 April 2014

9. J. R. Abernathey and F. Rosenberger, Time-Dependent Convective Instabilities in a Closed Vertical Cylinder Heated from Below, *J. Fluid Mech.*, vol. 160, pp. 137–154, 1985.
10. Y. Kamotani, F.-B. Weng, and S. Ostrach, Oscillatory Natural Convection of a Liquid Metal in Circular Cylinders, *J. Heat Transfer*, vol. 116, pp. 627–632, 1994.
11. J. P. Pulicani, S. Krukowski, J. I. D. Alexander, J. Ouazzani, and F. Rosenberger, Convection in an Asymmetrically Heated Cylinder, *Int. J. Heat Transfer*, vol. 35, pp. 2119–2130, 1992.
12. R. S. Feigelson and R. K. Route, Vertical Bridgman Growth of $CdGeAs_2$ with Control of Interface Shape and Orientation, *J. Cryst. Growth*, vol. 49, pp. 261–273, 1980.
13. P. S. Dutta, K. S. Sangunni, H. L. Bhat, and V. Kumar, Growth of Gallium Antimonide by Vertical Bridgman Technique with Planar Crystal-Melt Interface, *J. Cryst. Growth*, vol. 141, pp. 44–50, 1994.
14. K. Kakimoto, M. Eguchi, H. Watanabe, and T. Hibiya, Flow Instability of Molten Silicon in the Czochralski Configuration, *J. Cryst. Growth*, vol. 102, pp. 16–20, 1990.
15. K. Kakimoto, M. Watanabe, M. Eguchi, and T. Hibiya, Flow Instability of the Melt During Czochralski Si Crystal Growth: Dependence on Growth Conditions—A Numerical Simulation Study, *J. Cryst. Growth*, vol. 139, pp. 197–205, 1994.
16. W. E. Langlois, Buoyancy-Driven Flows in Crystal-Growth Melts, in M. V. Dyke (ed.), *Annual Review of Fluid Mechanics*, vol. 17, pp. 191–215, Annual Review Inc., Palo Alto, CA, 1985.
17. F. H. Harlow and J. E. Welch, Numerical Calculation of Time-Dependent Viscous Incompressible Flow of Fluid with Free Surface, *Phys. Fluids*, vol. 8, pp. 2182–2189, 1965.
18. S. V. Patankar, *Numerical Heat Transfer and Fluid Flow*, chap. 5, Hemisphere, Washington, D.C., 1980.
19. E. Haug and K. K. Choi, *Method of Engineering Mathematics*, p. 237, Prentice-Hall, Englewood Cliffs, N.J., 1993.

Downloaded by [National Chiao Tung University] at 05:50 28 April 2014